

B_{1g} -like pairing states in two-leg ladder iron superconductors

Weicheng Lv, Adriana Moreo, and Elbio Dagotto

*Department of Physics and Astronomy, University of Tennessee, Knoxville, Tennessee 37996, USA and
Materials Science and Technology Division, Oak Ridge National Laboratory, Oak Ridge, Tennessee 37831, USA*

(Dated: October 30, 2018)

Motivated by the recent report of superconductivity in Fe-based ladder materials, we study the pairing state of a multi-orbital t - J model defined on two-leg ladders using the standard mean-field theory. We find that the superconducting order parameters change sign between the d_{xz} and d_{yz} orbitals in most of the phase diagram. By analogy with the two-dimensional Fe planes, we conclude that the leading pairing channel of this state belongs to the B_{1g} symmetry class, which is distinct from the common s_{\pm} gap with the A_{1g} symmetry. By smoothly interpolating from planes into ladders, we show that a first-order transition occurs between these two competing phases when the dimension of the system is reduced.

PACS numbers: 74.70.Xa, 74.20.Rp

I. INTRODUCTION

Understanding the interplay between superconductivity and magnetism is the central topic in the study of unconventional superconductors.¹ In the context of the Fe-based materials several theories have been proposed based on the weak-coupling²⁻⁷ and strong-coupling⁸⁻¹² limits. In the former case, near the spin-density-wave instability the pairing interaction is mediated by the exchange of spin fluctuations between the hole and electron pockets. By contrast, theories that start in the strong-coupling limit argue that superconductivity arises as in doped Mott insulators, where the electron pairing is induced by the short-range magnetic exchanges between localized moments. These two scenarios predict the same s_{\pm} pairing state and are difficult to distinguish because the electrons in the Fe-based superconductors show both local and itinerant characters.¹³⁻¹⁸ To resolve this controversy, one alternative approach is to explore new materials that may share a universal pairing mechanism. Indeed, many significant insights have been gained from the recent studies of KFe_2As_2 that only has Fermi surface hole pockets¹⁹⁻²² and KFe_2Se_2 where only the electron pockets are present.²³⁻²⁸

In this regard, the very recent report²⁹ of possible superconductivity in the Fe-based two-leg ladder material $\text{K}_3\text{Fe}_4\text{Se}_6$ may provide a new testing ground for the existing theories. The actual sample of this material is made of a single layer of the bulk KFe_2Se_2 grown along the crystal [110] direction. The basic building block is the Fe_2Se_3 ladder, which consists of two parallel Fe chains that are strongly bound together, as shown in Fig. 1. These ladders are then weakly coupled to each other through layers of K atoms. In fact, the same Fe-based two-leg ladder structure has been realized previously in bulk materials BaFe_2Se_3 and KFe_2Se_3 , both of which are, however, insulators. It is interesting to note that in BaFe_2Se_3 and below $T_N \approx 256$ K, the Fe spins form 2×2 ferromagnetic (FM) blocks, which are antiferromagnetically (AFM) coupled along the chain direction.³⁰⁻³² For KFe_2Se_3 , below $T_N \approx 250$ K there also exists a dif-

ferent magnetic ground state³³ in which the spins are FM aligned on the same rung, but AFM ordered along the chain. Furthermore, both materials exhibit very large ordered moments, ranging from $2.8 \mu_B$ per Fe in BaFe_2Se_3 to $2.1 \mu_B$ in KFe_2Se_3 . Assuming a valence +1 for K and -2 for Se, we find that superconducting $\text{K}_3\text{Fe}_4\text{Se}_6$ has the Fe valence of +2.25, which lies between +2 of BaFe_2Se_3 and +2.5 of KFe_2Se_3 . Therefore superconductivity in these Fe-ladder materials appears to arise from doping AFM insulators, which locates them closer to the high- T_c copper-oxide superconductors than the earlier Fe-based pnictide superconductors.

In the context of the cuprates, extensive research has been carried out for the one-band model on two-leg ladders.³⁴⁻³⁷ It has been well established that in the undoped limit there is a spin gap due to the particular ladder geometry, and that upon doping superconductivity mainly occurs in the d -wave channel.³⁸ Both features are also found in the layered cuprates that are composed of two-dimensional CuO_2 planes. So it is very interesting to study whether such a remarkable similarity between the two-leg ladders and the two-dimensional planes for the case of the cuprates also exists in the multi-orbital Fe-based superconductors.

The magnetic properties of the Fe ladders have been investigated theoretically using both first principles³⁹ and model calculations.⁴⁰ In this work, the pairing state of these materials will be studied. Because the parent compounds are insulators with high Néel temperature and large ordered moment, in this publication we will follow the strong-coupling approach, in particular, the mean-field theory of a multi-orbital t - J model on two-leg ladders. We emphasize that, by definition of the strong-coupling theory, the t - J model should be derived from some Hubbard model in the limit of large on-site interaction U . However, such procedure is very complicated due to the multi-orbital nature of the Fe-based superconductors. Therefore, our current study and other earlier works^{9,11,24,25} simply start from a phenomenological t - J model by assuming the existence of the local moments. Our main result is that the superconducting phase of the

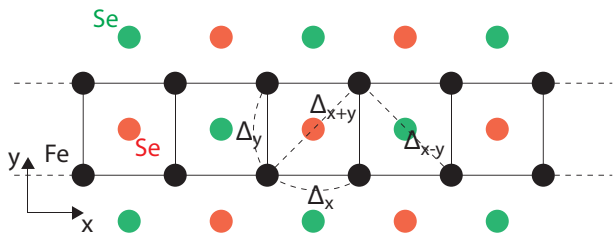


FIG. 1. (Color online) Schematic illustration of the two-leg ladder iron selenides. The Se atoms are located either above (red) or below (green) the Fe plane. x and y label the directions of the chain and rung, respectively. Δ_x , Δ_y , Δ_{x+y} , Δ_{x-y} are the superconducting order parameters with the pair of electrons located in nearest neighbors (NN) sites along the chain or rung, or involving next nearest neighbors (NNN) sites, respectively.

Fe ladders belongs to a different symmetry class from that of the two-dimensional Fe planes. When dimension is reduced from planes to ladders, the system undergoes a first-order transition between the two phases. The paper is organized as follows. First, the basic formulations are outlined in Sec. II. The main results are shown in Sec. III. In particular, the isolated Fe ladder is considered in Sec. III A whereas Sec. III B studies the nontrivial evolution from planes to ladders using a model system of coupled ladders. Finally Sec. IV concludes the publication with a discussion of results and a brief summary.

II. MULTI-ORBITAL t - J MODEL ON LADDERS

Let us first define the multi-orbital t - J model on a two-leg ladder,

$$\mathcal{H} = \mathcal{H}_K + \mathcal{H}_J. \quad (1)$$

\mathcal{H}_K is the kinetic energy, represented by a tight-binding model,

$$\mathcal{H}_K = \sum_{\langle \mathbf{r}, \mathbf{r}' \rangle} \sum_{\alpha\beta, s} \left(t_{\mathbf{r}\mathbf{r}'}^{\alpha\beta} c_{\mathbf{r}\alpha s}^\dagger c_{\mathbf{r}'\beta s} + h.c. \right) - \mu \sum_{\mathbf{r}, \alpha} n_{\mathbf{r}}^\alpha, \quad (2)$$

where $c_{\mathbf{r}\alpha s}^\dagger$ creates an electron at site \mathbf{r} on orbital α with spin s . The density operator is $n_{\mathbf{r}}^\alpha = \sum_s c_{\mathbf{r}\alpha s}^\dagger c_{\mathbf{r}\alpha s}$, and μ is the chemical potential. Because our model is defined on a two-leg ladder as illustrated in Fig. 1, the site index \mathbf{r} has two components, $\mathbf{r} = (m, i)$, where $m = 1, 2$ labels the two parallel chains and i is the site index on each chain. It should also be noted that the whole system does not have the full translational symmetry of the Fe ladder along the x (chain) direction due to the staggered positions of the Se atoms (Fig. 1). The real unit cell of the Fe_2Se_3 ladder contains four Fe sites. However, similarly as carried out in higher-dimensional systems,^{41–44} we can perform a gauge transformation, $c_{\mathbf{r}\alpha s} \rightarrow \exp(i\mathbf{K} \cdot \mathbf{r}) c_{\mathbf{r}\alpha s}$ for $\alpha = d_{xy}, d_{x^2-y^2}, d_{3z^2-r^2}$, where $\mathbf{K} = (\pi, \pi)$. After such a transformation, the

tight-binding model \mathcal{H}_K (2) becomes invariant under the translation by one Fe lattice spacing along the x (chain) direction. Therefore, we can work in the effective unit cell that contains only two Fe sites along the rung. The hopping parameters $t_{\mathbf{r}\mathbf{r}'}^{\alpha\beta}$ are taken from the earlier three-orbital model⁴³ with d_{xz} , d_{yz} , and d_{xy} orbitals. In principle, due to the ladder geometry, these parameters can have different values here.⁴⁰ Especially, the hopping amplitudes along the x (chain) direction are not necessarily the same as those along the y (rung) direction. The on-site energies of the d_{xz} and d_{yz} orbitals should also be different. However, for the purpose of simplicity, we use the same set of parameters derived for the two-dimensional Fe planes in Ref. 43. Namely, the tight-binding parameters themselves retain the C_4 rotational symmetry of the square lattice, and it is the geometry of the ladder that induces the symmetry breaking. This procedure will facilitate the discussion on the evolution of the superconducting state from planes to ladders. We also note that the band structure of the Fe ladder in our model, as shown in Fig. 2, is different from that obtained by the first-principles calculation in Ref. 29. However, while our main conclusion, i.e. the appearance of the B_{1g} pairing state in ladders, may depend on the particular hopping parameters chosen here, our main goal is to show that at least in *one* case a change in pairing symmetry can occur in the interpolation from planes to ladders. Developing a more refined set of parameters from first-principles calculations would not be appropriate considering that the many-body techniques employed here are based on the strong-coupling limit. Finally we set the chemical potential μ to give an electron filling $n = 3.75$ per site, which corresponds to 0.25 hole doping as in the superconducting Fe-ladder material $\text{K}_3\text{Fe}_4\text{Se}_6$.

\mathcal{H}_J is the exchange energy between the spins on the neighboring sites,

$$\mathcal{H}_J = \sum_{\langle \mathbf{r}, \mathbf{r}' \rangle} \sum_{\alpha\beta} J_{\mathbf{r}\mathbf{r}'}^{\alpha\beta} \left(\mathbf{S}_{\mathbf{r}}^\alpha \cdot \mathbf{S}_{\mathbf{r}'}^\beta - \frac{1}{4} n_{\mathbf{r}}^\alpha n_{\mathbf{r}'}^\beta \right), \quad (3)$$

where the spin operator is $\mathbf{S}_{\mathbf{r}}^\alpha = 1/2 \sum_{ss'} c_{\mathbf{r}\alpha s}^\dagger \boldsymbol{\sigma}_{ss'} c_{\mathbf{r}\alpha s'}$, with $\boldsymbol{\sigma}$ being the Pauli matrix. Similarly as in earlier work,⁸ the superexchanges are restricted to involve only the nearest-neighbors (NN), J_1 , and the next-nearest-neighbors (NNN), J_2 . It is further assumed that the NN exchanges are isotropic between the bonds along the chain and those along the rung, $J_{1x} = J_{1y} = J_1$, which does not necessarily hold for the ladder geometry but our intention is to reduce to the minimum the number of free parameters in the model.

Following the standard procedure,^{9,11,24,25} we define the singlet pairing operators between the sites \mathbf{r} and \mathbf{r}' ,

$$P_{\mathbf{r}\mathbf{r}'}^{\alpha\beta} = c_{\mathbf{r}\alpha\uparrow} c_{\mathbf{r}'\beta\downarrow} - c_{\mathbf{r}\alpha\downarrow} c_{\mathbf{r}'\beta\uparrow}, \quad (4)$$

and express the exchange energy \mathcal{H}_J in terms of $P_{\mathbf{r}\mathbf{r}'}^{\alpha\beta}$,

$$\mathcal{H}_J = - \sum_{\langle \mathbf{r}, \mathbf{r}' \rangle} \sum_{\alpha\beta} \frac{J_{\mathbf{r}\mathbf{r}'}^{\alpha\beta}}{2} \left(P_{\mathbf{r}\mathbf{r}'}^{\alpha\beta} \right)^\dagger P_{\mathbf{r}\mathbf{r}'}^{\alpha\beta}. \quad (5)$$

Then, \mathcal{H}_J can be decoupled by the standard mean-field theory in the pairing channel. The superconducting order parameters between orbitals α and β at sites \mathbf{r} and \mathbf{r}' are defined as

$$\Delta_{\mathbf{r}\mathbf{r}'}^{\alpha\beta} = J_{\mathbf{r}\mathbf{r}'}^{\alpha\beta} \langle P_{\mathbf{r}\mathbf{r}'}^{\alpha\beta} \rangle. \quad (6)$$

For the J_1 - J_2 model used here, assuming translational symmetry, we can identify four distinct order parameters for each orbital pair (α, β), namely Δ_x and Δ_y between NN sites along the chain and rung, and Δ_{x+y} and Δ_{x-y} between NNN sites, as shown in Fig. 1. After the standard Fourier transform, we have the following BCS mean-field Hamiltonian,

$$\begin{aligned} \mathcal{H}_{MF} = & \sum_{k,mn,\alpha\beta,s} (\varepsilon_{mn}^{\alpha\beta}(k) - \mu\delta_{\alpha\beta}\delta_{mn}) c_{km\alpha s}^\dagger c_{kn\beta s} \\ & + \sum_{k,mn,\alpha\beta} \left(\Delta_{mn}^{\alpha\beta}(k) c_{km\alpha\uparrow}^\dagger c_{-kn\beta\downarrow}^\dagger + h.c. \right). \end{aligned} \quad (7)$$

Such a model can be solved self-consistently. In general, with different initial conditions, there are many self-consistent solutions, of which we choose the one that minimizes the ground state energy,^{11,24,25}

$$\mathcal{E} = \sum_{\langle \mathbf{r}, \mathbf{r}' \rangle} \sum_{\alpha\beta} \frac{1}{2J_{\mathbf{r}\mathbf{r}'}^{\alpha\beta}} \left| \Delta_{\mathbf{r}\mathbf{r}'}^{\alpha\beta} \right|^2 - \sum_{k,n} (E_{k,n} - \varepsilon_{k,n} + \mu). \quad (8)$$

$E_{k,n}$ are the quasiparticle energies obtained from the diagonalization of the BCS mean-field Hamiltonian \mathcal{H}_{MF} (7), whereas $\varepsilon_{k,n}$ are the band dispersions of the tight-binding model \mathcal{H}_K (2). In order to limit the number of parameters, we assume that the superexchanges J are orbitally diagonal and orbitally independent, namely $J_{\mathbf{r}\mathbf{r}'}^{\alpha\beta} = \delta_{\alpha\beta} J_{\mathbf{r}\mathbf{r}'}$. Therefore the pairing only occurs within the same orbitals, $\Delta_{\mathbf{r}\mathbf{r}'}^{\alpha\beta} = \delta_{\alpha\beta} \Delta_{\mathbf{r}\mathbf{r}'}(\alpha)$. The case in which the intra-orbital and inter-orbital superexchanges are of equal strength has also been studied. Similar to earlier works,^{11,24} the inclusion of the inter-orbital pairings, which are found to be much smaller than the intra-orbital ones, does not change the results qualitatively at least within the approximations used here. Thus, for simplicity, we will only focus on the intra-orbital pairing arising from orbitally diagonal superexchange interactions in this article.

III. RESULTS

A. Isolated ladders

Let us consider first a single Fe ladder as shown in Fig. 1. Periodic and open boundary conditions are imposed along the chain and rung directions, respectively. The band dispersions $\varepsilon_{k,n}$ along the x (chain) direction are plotted in Fig. 2 with the colors denoting the dominant orbital contributions. From now on, the implicit energy unit of eV will be used unless noted otherwise. Since

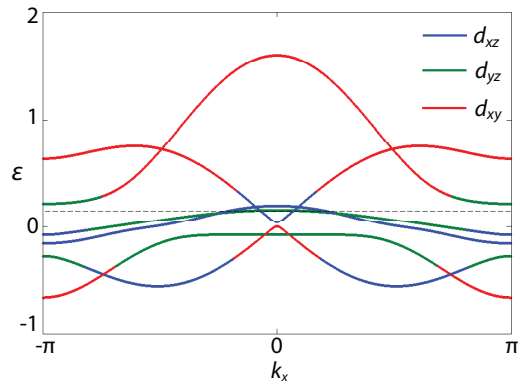


FIG. 2. (Color online) Band dispersions along the x (chain) direction. The colors correspond to the dominant orbital contributions, d_{xz} (blue), d_{yz} (green), and d_{xy} (red). The horizontal dashed line denotes the chemical potential for filling $n = 3.75$.

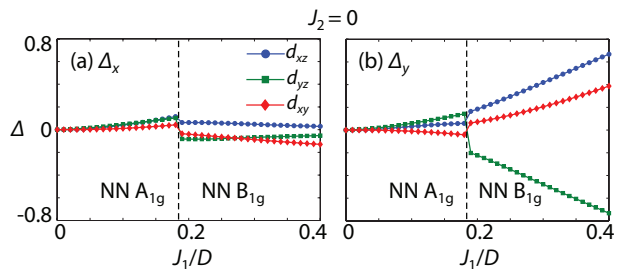


FIG. 3. (Color online) Superconducting order parameters (a) Δ_x and (b) Δ_y for each orbital as functions of the NN exchange J_1 for the case of the NNN exchange $J_2 = 0$. D is the bandwidth. The vertical dashed line marks the first-order transition between the two phases, i.e. NN A_{1g} and NN B_{1g} .

the effective unit cell contains two Fe sites along the y (rung) direction, there are six bands in the present three-orbital model. As discussed earlier, we have set the chemical potential at the filling level $n = 3.75$, corresponding to 0.25 hole doping. Apparently, no nesting instability can be identified, with the d_{xz} and d_{yz} orbitals dominating the states at the Fermi energy. Because the ladder structure explicitly breaks the symmetry of the two-dimensional square lattice, one cannot rigorously categorize the pairing state by the one-dimensional representation of the D_{4h} point group, as in earlier efforts.^{11,24,25,43} For ladders it is necessary to study each of the superconducting order parameters $\Delta_{\mathbf{r}\mathbf{r}'}(\alpha)$ separately. However, in order to compare the ladders with the planes, we will attempt to identify approximately the leading pairing symmetry by analogy with the two-dimensional case.

As the first step, let us set the NNN exchange J_2 to zero and consider only the NN pairing induced by J_1 . In Fig. 3, the superconducting order parameters between NN sites along the x (chain) and y (rung) directions, Δ_x and Δ_y , are shown for each of the three orbitals as functions of J_1 . The coupling J_1 is measured in units of

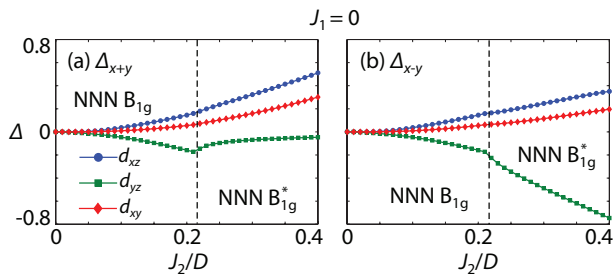


FIG. 4. (Color online) Superconducting order parameters (a) Δ_{x+y} and (b) Δ_{x-y} for each orbital as functions of the NNN exchange J_2 for the case of the NN exchange $J_1 = 0$. D is the bandwidth. The vertical dashed line marks the second-order transition between the two phases, i.e. NNN B_{1g} ($\Delta_{x+y} = \Delta_{x-y}$) and NNN B_{1g}^* ($\Delta_{x+y} \neq \Delta_{x-y}$).

the bandwidth D . Two different regimes can be identified as J_1 is varied. When $J_1 \lesssim 0.18D$, Δ_x and Δ_y have comparable amplitudes. In particular, they take the same sign on the d_{xz} and d_{yz} orbitals (s -wave) whereas they have different signs (d -wave) on d_{xy} . At first sight, it is difficult to assign the pairing symmetry for such a state because different symmetries occur on different orbitals. However, we note that the electrons in the vicinity of the Fermi energy are mostly from the d_{xz} and d_{yz} orbitals (Fig. 2). Consequently the superconducting gaps on these two orbitals are larger than the gap on d_{xy} so that the system can gain more condensation energy. Therefore, we can approximately categorize the pairing symmetry as A_{1g} according to the gap structure restricted to the d_{xz} and d_{yz} orbitals. However, note that when $J_1 \gtrsim 0.18D$, the system evolves into a second phase through a first-order transition. The superconducting gap remains s -wave on d_{xz} and d_{yz} , and d -wave on d_{xy} . But unlike the previous case, $\Delta(d_{xz})$ and $\Delta(d_{yz})$ now display opposite signs. We recall that the overall pairing symmetry of a multi-orbital system depends on both the spatial and orbital gap structures.^{11,24,25,43} Therefore, by analogy with the two-dimensional planes, this phase belongs to the B_{1g} symmetry class due to the sign difference between $\Delta(d_{xz})$ and $\Delta(d_{yz})$. As J_1 further increases, Δ_x gets strongly suppressed while Δ_y becomes the leading pairing channel. This result can be understood from the earlier work on the one-band model in the context of the cuprates.³⁴⁻³⁷ In the large J_1 limit, the undoped system has a spin-liquid ground state in which the spins tend to form local singlets on the same rung. When holes are doped into the system, they prefer to occupy the sites on the same rung because such a state has the lowest energy by breaking the fewest local singlets. Therefore, the pairing mainly occurs in the Δ_y channel along the rung when J_1 is large. Here we have found similar results using a multi-orbital model.

Now let us consider the other limit, namely the case where the NN exchange is zero, $J_1 = 0$, and the pairing occurs between the NNN sites. Figure 4 shows the NNN superconducting order parameters Δ_{x+y} and Δ_{x-y}

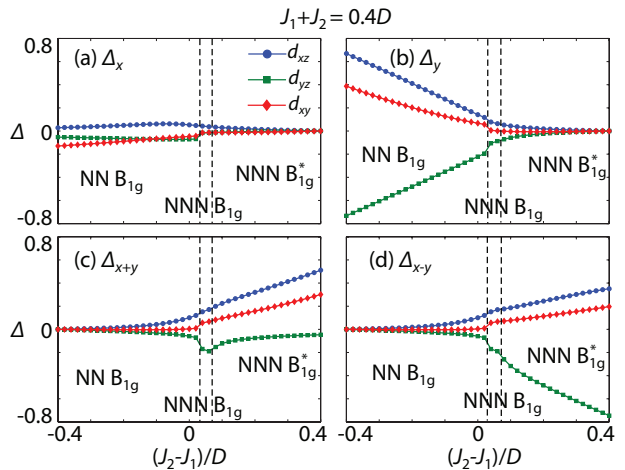


FIG. 5. (Color online) Superconducting order parameters (a) Δ_x , (b) Δ_y , (c) Δ_{x+y} , and (d) Δ_{x-y} for each orbital as functions of the difference between the NNN and NN exchanges, $J_2 - J_1$. The sum of J_1 and J_2 is fixed to be $0.4D$, where D is the bandwidth. The vertical dashed lines separate the three phases, NN B_{1g} , NNN B_{1g} , and NNN B_{1g}^* .

as functions of J_2 . In this case there are two different phases stabilized at the small and large J_2 limits, respectively. When $J_2 \lesssim 0.21D$, the two NNN gaps are equal (s -wave) for each of the three orbitals. Similarly to the previous case, we identify the dominant pairing symmetry by the gap structure on the leading d_{xz} and d_{yz} orbitals. Because $\Delta_{x\pm y}$ have opposite signs on d_{xz} and d_{yz} , the B_{1g} symmetry is assigned to this phase. When $J_2 \gtrsim 0.21D$, Δ_{x+y} and Δ_{x-y} now have different values, which suggests a mixture phase with both s - and d -wave components. Similar results with $\Delta_{x+y} \neq \Delta_{x-y}$ have also been found in the study of the two-dimensional Fe planes in the large J_2 limit.^{24,25} It is important to emphasize that B_{1g} is still the dominant pairing symmetry here although other gap amplitudes with different symmetries also take significant values. Consequently, this phase is labeled as B_{1g}^* to distinguish it from the previous B_{1g} phase at $J_2 \lesssim 0.21D$. In contrast to the first-order transition from the NN A_{1g} to NN B_{1g} states observed in Fig. 3, here the leading pairing symmetry does not change between the NNN B_{1g} and NNN B_{1g}^* phases, and thus the transition occurs smoothly, as shown in Fig. 4. Finally, we recall that in the earlier works^{9,11,24,25} for the two-dimensional Fe planes, the NNN J_2 coupling consistently led to the s_{\pm} gap with the A_{1g} symmetry, in which the NNN superconducting order parameters are equal not only on the two NNN bonds, but also on the two orbitals of d_{xz} and d_{yz} , i.e. $\Delta_{x\pm y}(d_{xz}) = \Delta_{x\pm y}(d_{yz})$. Consequently, in our calculations the pairing symmetry of the planes is fundamentally different from that of the two-leg ladders, where a sign change occurs between the superconducting order parameters on d_{xz} and d_{yz} . This nontrivial dimensional crossover from planes to ladders will be studied in detail in Sec. III B.

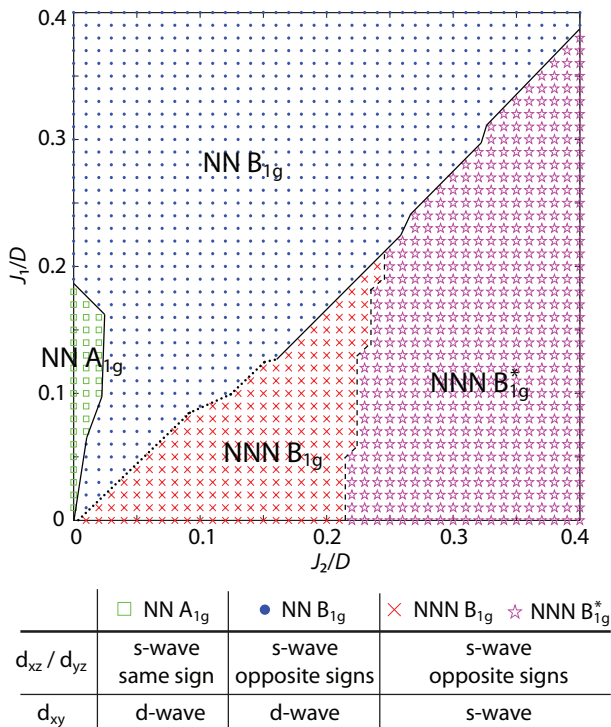


FIG. 6. (Color online) The superconducting phase diagram of the isolated Fe ladders as a function of J_1 and J_2 , both measured in units of the bandwidth D . Different symbols correspond to different phases determined by the leading pairing symmetries. The solid line marks a first-order transition; the dashed line represents a second-order transition; and the dotted line illustrates the crossover between the NN B_{1g} and the NNN B_{1g} phases at small J .

Thus far, we have observed that two different phases, the NN B_{1g} state dominated by the rung pairing Δ_y and the NNN B_{1g}^* state with $\Delta_{x+y} \neq \Delta_{x-y}$, are stabilized at the limits of large J_1 and large J_2 , respectively. It will be interesting to investigate how the two phases compete with each other when both J_1 and J_2 are nonzero. For this purpose, let us fix the sum of J_1 and J_2 to be $J_1 + J_2 = 0.4D$, and plot each of the four superconducting order parameters as a function of $J_2 - J_1$ in Fig. 5. In this case, we observe that the NN rung pairing Δ_y is still the dominant pairing channel even when a small but finite J_2 is turned on. This NN B_{1g} phase extends up to the parameter space with $J_2 - J_1 \lesssim 0.03D$. Then, the system transitions into the NNN B_{1g} state with $\Delta_{x+y} = \Delta_{x-y}$ when $0.03D \lesssim J_2 - J_1 \lesssim 0.07D$, before the B_{1g}^* phase ($\Delta_{x+y} \neq \Delta_{x-y}$) becomes the ground state at $J_2 - J_1 \gtrsim 0.07D$. It is clear from Fig. 5 that the transition between the NN B_{1g} and the NNN B_{1g} states is characterized by a discontinuous jump of the order parameters. However, because the two phases belong to the same B_{1g} symmetry class, the transition is not always first order and a smooth crossover does occur at smaller superexchanges J (results not shown here).

Finally, we have systematically studied the ground

state of the system as a function of J_1 and J_2 by varying each of those couplings from 0 to $0.4D$. The phase diagram, which is determined by the leading pairing symmetries, is shown in Fig. 6. We find that the NN A_{1g} phase, which was observed at $J_1 \lesssim 0.18D$ with $J_2 = 0$ (Fig. 3), only exists in a limited region with very small NNN exchange $J_2 \lesssim 0.03D$. Instead, the phase diagram is dominated by the NN B_{1g} and the NNN B_{1g} (B_{1g}^*) phases, which are separated approximately by the line $J_1 \approx J_2$. When $J \gtrsim 0.16D$ (solid line), the transition between the two phases is first order as shown in Fig. 5. The intermediate NNN B_{1g} phase disappears for $J \gtrsim 0.25D$, where a direct transition occurs between the NN B_{1g} and NNN B_{1g}^* phases. Furthermore, the NNN B_{1g} and NNN B_{1g}^* states are separated by a nearly vertical dashed line around $J_2 \approx 0.23D$, where a second-order phase transition takes place with a smooth onset of the pairing amplitudes with different symmetries. As discussed previously, the pairing symmetry does not change from the NN B_{1g} to the NNN B_{1g} states. Consequently the transition between the two phases is not necessarily first order. Indeed, when $J \lesssim 0.16D$, we do observe a crossover transition (dotted line), where the superconducting order parameters exhibit continuous changes. By contrast, a first-order transition (solid line) always occur between the NN A_{1g} and NN B_{1g} phases, which belong to different symmetry classes.

B. Coupled ladders

As the discussions in Sec. III A have shown, for the two-leg Fe ladders, B_{1g} is the dominant pairing symmetry and the superconducting order parameters have opposite signs on the d_{xz} and d_{yz} orbitals. On the other hand, for the two-dimensional Fe planes,^{9,11,24,25} the NNN exchange J_2 consistently produces the s_{\pm} gap with the A_{1g} symmetry, which requires $\Delta_{x\pm y}(d_{xz}) = \Delta_{x\pm y}(d_{yz})$. Apparently, the superconducting states of the Fe ladders and the Fe planes are fundamentally different.

In this section, we will study how this change of symmetry occurs as the system evolves from planes to ladders. For this purpose, let us consider the model system shown in Fig. 7. It is a two-dimensional square lattice consisting of $N \times N$ sites with periodic boundary conditions in both directions. Translational symmetry is imposed along the x direction, while strong and weak bonds occur in staggered order along the y direction. Then, essentially we have $N/2$ parallel two-leg ladders that are weakly coupled to their neighbors. We use t and J for the intra-ladder hopping amplitudes and superexchanges, and t' and J' for the inter-ladder ones. For simplicity, we have chosen $t' = \eta t$ and $J' = \eta J$, where the ratio η is a single parameter representing the relative strength of the inter-ladder couplings with respect to the intra-ladder ones. In the limit of $\eta = 1$, the system becomes an isotropic two-dimensional square lattice, which has been extensively studied in earlier works.^{9,11,24,25} When $\eta = 0$,

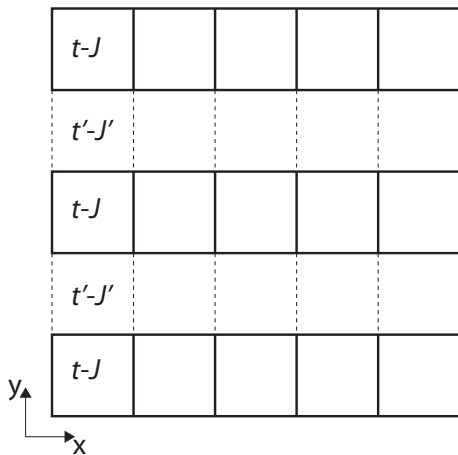


FIG. 7. Illustration of the coupled ladders used here. The system consists of two-leg ladders aligned along the x direction (solid lines). These ladders are coupled along the y direction through weaker inter-ladder couplings (dashed lines). t (t') and J (J') are intra-ladder (inter-ladder) hopping amplitudes and exchange constants, respectively.

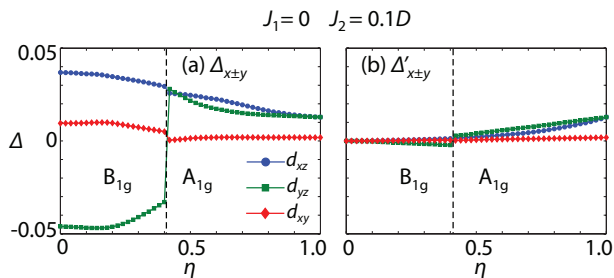


FIG. 8. (Color online) The NNN intra-ladder and inter-ladder superconducting order parameters, (a) $\Delta_{x\pm y}$ and (b) $\Delta'_{x\pm y}$, for each orbital as functions of the relative coupling strength parameter η . The exchange constants are fixed to values $J_1 = 0$ and $J_2 = 0.1D$. The vertical dashed line marks the first-order transition between the A_{1g} phase of the planes and the B_{1g} phase of the ladders.

the system reduces to $N/2$ isolated ladders that were considered previously in Sec. III A. By varying η from 1 to 0, we can tune the system continuously from two-dimensional planes to two-leg ladders, and study how superconductivity evolves. As the band dispersion changes with η , the chemical potential μ needs to be adjusted accordingly so that the filling level is always fixed at $n = 3.75$. The exchange constants J_1 and J_2 are always measured in units of D , the bandwidth of the isolated ladders.

Let us first consider the role played by the NNN exchange J_2 by setting the NN exchange to $J_1 = 0$. The superconducting order parameters at $J_2 = 0.1D$ are plotted as functions of η in Fig. 8, with Δ and Δ' representing the intra-ladder and inter-ladder pairing strengths, respectively. For the parameters used here, we always have $\Delta_{x+y} = \Delta_{x-y}$ and $\Delta'_{x+y} = \Delta'_{x-y}$, so only one of each is

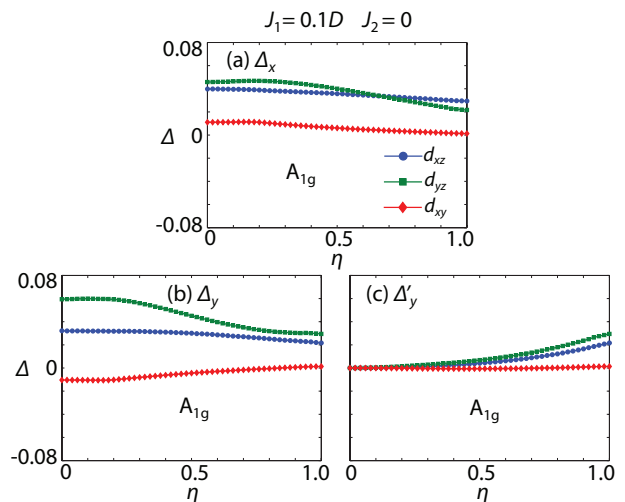


FIG. 9. (Color online) The NN intra-ladder and inter-ladder superconducting order parameters, (a) Δ_x , (b) Δ_y , and (c) Δ'_y for each orbital as functions of the relative coupling strength parameter η . The exchange constants are fixed to values $J_1 = 0.1D$ and $J_2 = 0$. In this case the system transitions smoothly from planes to ladders, where A_{1g} is always the dominant pairing symmetry.

shown. As it can be observed from Fig. 8, when $\eta = 1$ the intra-ladder and the inter-ladder pairing strengths are equal, i.e. $\Delta_{x\pm y} = \Delta'_{x\pm y}$, which preserves the translational symmetry along the y direction. Furthermore, these superconducting order parameters take the same value on the d_{xz} and d_{yz} orbitals. Such a state belongs to the A_{1g} symmetry class, with the pairing structural factor $\cos k_x \cos k_y$, in agreement with earlier studies.^{11,24,25} When η is reduced, the translational symmetry along the y direction is now explicitly broken, with the intra-ladder pairing being enhanced and the inter-ladder one being reduced. But $\Delta_{x\pm y}(d_{xz})$ and $\Delta_{x\pm y}(d_{yz})$ still have the same sign as long as $\eta \gtrsim 0.41$. Across $\eta \approx 0.41$, the system undergoes a discontinuous transition from the A_{1g} phase into the B_{1g} phase, where the signs of $\Delta_{x\pm y}(d_{xz})$ and $\Delta_{x\pm y}(d_{yz})$ suddenly become opposite. Then the system evolves continuously into the state of the isolated ladders that was previously discussed at $\eta = 0$. Indeed the superconducting phases of the two-dimensional planes and two-leg ladders belong to different symmetry classes. So the system does not evolve smoothly from planes to ladders, but a first-order transition separates the two competing phases.

Now we focus on the NN pairings by setting $J_1 = 0.1D$ and $J_2 = 0$. The results are shown in Fig. 9, where the intra-ladder Δ_x , Δ_y and the inter-ladder Δ'_y are displayed. Again at $\eta = 1$, the intra-ladder and inter-ladder pairings are equal, $\Delta_y = \Delta'_y$. Furthermore, on the d_{xz} and d_{yz} orbitals, we have $\Delta_x(d_{xz}) = \Delta_y(d_{yz})$ and $\Delta_x(d_{yz}) = \Delta_y(d_{xz})$. Then, this state also belongs to the A_{1g} symmetry class with the leading structural factor $\cos k_x + \cos k_y$. Similarly to the previous case,

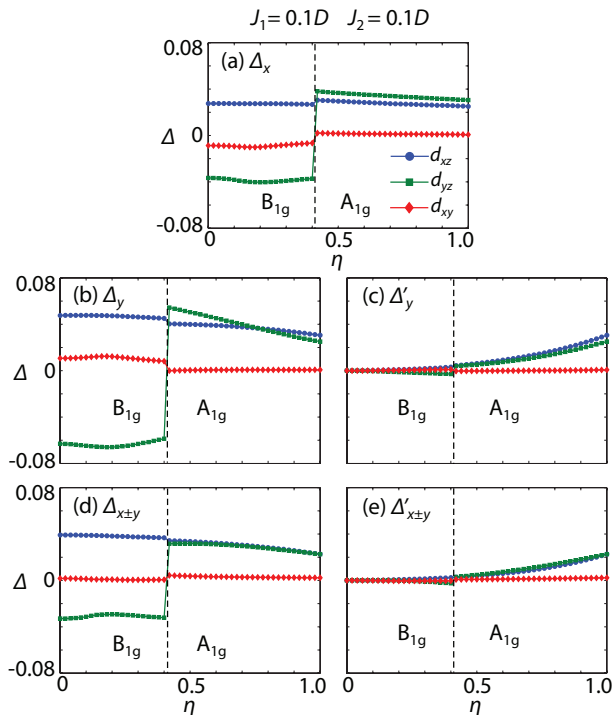


FIG. 10. (Color online) The superconducting order parameters, (a) Δ_x , (b) Δ_y , (c) Δ'_y , (d) $\Delta_{x\pm y}$, and (e) $\Delta'_{x\pm y}$ for each orbital as functions of the relative coupling strength parameter η . The exchange constants have been set to $J_1 = 0.1D$ and $J_2 = 0.1D$. The vertical dashed line marks the first-order transition between the A_{1g} phase of the planes and the B_{1g} phase of the ladders.

when η is reduced the intra-ladder pairings are enhanced while the inter-ladder ones are suppressed. However, we do not observe any discontinuity as η varies from 1 to 0, which suggests that the superconducting phase of the planes and that of the ladders are smoothly connected with one another. Actually, as shown by Fig. 3, the leading pairing channel of the two-leg ladders also has the A_{1g} symmetry at $J_1 = 0.1D$. Then, the evolution from planes to ladders is continuous without modifications of the pairing symmetry. However, it should be noted that the superconducting order parameter on the d_{xy} orbital does change from s -wave in the planes to d -wave in the ladders. But this symmetry change on the d_{xy} orbital only occurs continuously because the pairing symmetry is mostly determined by the gap structures on the d_{xz} and d_{yz} orbitals, which dominate the states around the Fermi energy.

Finally, let us study the case in which both J_1 and J_2 are present. Figure 10 shows all five independent superconducting order parameters as functions of η at fixed $J_1 = J_2 = 0.1D$. According to the phase diagram in Fig. 6, for the isolated ladders at $\eta = 0$, the ground state is a mixture of the NN B_{1g} phase and the NNN B_{1g} phase ($\Delta_{x+y} = \Delta_{x-y}$), both of which are characterized by opposite signs of $\Delta(d_{xz})$ and $\Delta(d_{yz})$. By contrast, for the

isotropic planes at $\eta = 1$, the system belongs to the A_{1g} symmetry class with both the NN and NNN pairings. As explained earlier, the evolution from planes to ladders cannot be smooth due to the symmetry change as η varies. Indeed our calculation results in Fig. 10 confirmed this prediction, with a sharp first-order transition occurring at $\eta \approx 0.41$. Furthermore, as the phase diagram in Fig. 6 shows, in most portions of the J_1 - J_2 phase diagram, B_{1g} is the leading pairing symmetry of the two-leg Fe ladders. The NN A_{1g} phase only occupies a limited portion, where the values of J_1 and J_2 are likely outside the physically relevant regime for the Fe-based superconductors. Then, it can be concluded that the evolution from planes to ladders in the model for Fe-based superconductors considered here occurs through a first-order transition with a nontrivial modification of the pairing symmetry.

Before ending this subsection, it is important to point out that our analysis is restricted to the case of small superexchanges J , where the ground state of the superconducting Fe planes automatically preserves the translational symmetry along the y direction. Namely, we always have $\Delta = \Delta'$ at $\eta = 1$ although they are treated as independent variables. However, when J becomes sufficiently large, an inhomogeneous solution with $\Delta \neq \Delta'$ was found to have a lower energy, spontaneously breaking the translation symmetry along the y direction at $\eta = 1$. We believe that this “stripe”-like state is nevertheless an artifact of the two-site unit cell used in our calculation. In fact, by enlarging the unit cell to a 2×2 plaquette, we have observed that the favorable solution becomes a checkerboard state, which breaks the translational symmetry along both x and y , but preserves the C_4 rotational symmetry. It is certainly possible that further inhomogeneous solutions with lower energies can be found if we keep enlarging the unit cell. More importantly, the gap amplitude of these inhomogeneous states is of order 0.1 eV (see Fig. 5 as a reference), which is unphysically large as compared to the gaps observed experimentally. Furthermore, with such a large superconducting gap, not only the electrons in the vicinity of the Fermi energy, but also those far away from it, participate in the pairing process and contribute significantly to the condensation energy. Therefore, the argument that the Fermi surface needs to match the gap structural factor⁴⁵ does not apply here. As a consequence, it is justified that our focus is only on the case of small exchanges J , in which the gap amplitudes, being of the order of 0.01 eV, are comparable to the experimental values.

IV. DISCUSSION AND SUMMARY

In Sec. III, it has been shown that the superconducting state of the two-leg Fe ladders is dominated by the B_{1g} phase, instead of the A_{1g} phase found in the two-dimensional Fe planes. But as it is well known, the superconducting order parameter of the B_{1g} phase is required

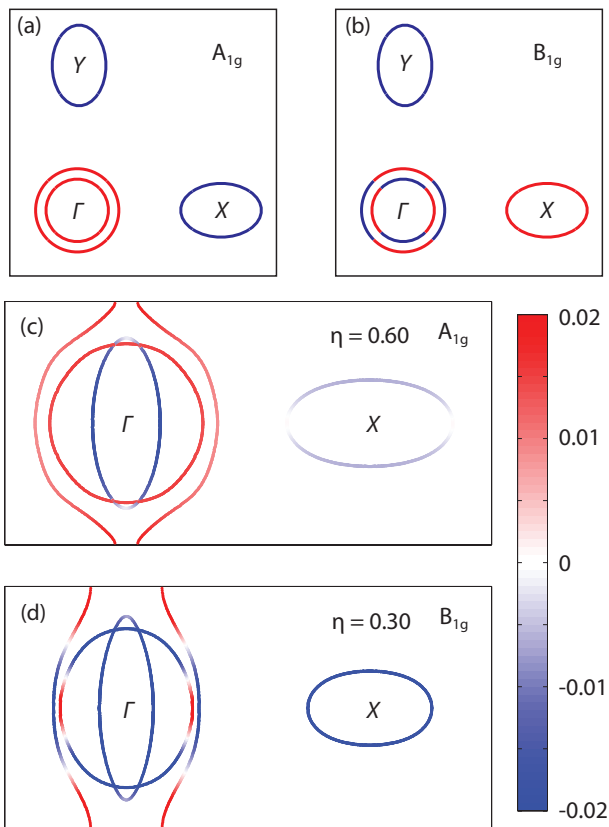


FIG. 11. (Color online) (a, b) Illustration of the superconducting order parameters $\Delta(k)$ on the Fermi surfaces of the two-dimensional Fe planes. Although (a) and (b) are schematic, they are close to the Fermi surfaces for the model used here. (a) A_{1g} symmetry. $\Delta(k)$ is positive (red) on the two hole pockets at Γ , and negative (blue) on the two electron pockets at X and Y . (b) B_{1g} symmetry. $\Delta(k)$ changes sign under a $\pi/2$ rotation, with gap nodes on the hole pockets. (c, d) The calculated superconducting order parameters $\Delta(k)$ on the Fermi surface of the coupled two-leg iron ladders. (c) The A_{1g} phase at $\eta = 0.6$. (d) The B_{1g} phase at $\eta = 0.3$. The same exchange parameters as in Fig. 8 have been used, i.e. $J_1 = 0$ and $J_2 = 0.1D$, with the critical coupling strength being $\eta_c \approx 0.41$.

to change sign under a $\pi/2$ rotation and gap nodes will always appear on the hole pockets at the zone center [Fig. 11(b)]. Consequently the B_{1g} state usually has a higher energy than the nodeless A_{1g} state [Fig. 11(a)]. So why does the B_{1g} symmetry become the favorable pairing channel in the Fe-based ladders?

To understand this curious result, let us consider the effect introduced by an infinitesimal change of η from the isotropic limit of $\eta = 1$. This perturbation hybridizes the states separated by the momentum $(0, \pi)$ and effectively folds the Brillouin zone along the line $k_y = \pm\pi/2$. For the general Fermi surface topology of the Fe-based superconductors [see Fig. 11(a) or (b)], the electron pocket at Y will overlap with the hole pockets at Γ upon folding. As it can be seen from Fig. 11(a), because the supercon-

ducting order parameters of the A_{1g} state have opposite signs on the hole and electron pockets, this hybridization generally reduces the gap amplitudes and increases the energy of the system. By contrast, for the B_{1g} state as shown in Fig. 11(b), gap nodes already exist on the hole pockets. The hybridization between the hole and electron pockets will not induce additional nodes, and thus the condensation energy of the system will remain the same up to the zeroth order. As a result, as the Fe plane is decoupled into the two-leg ladders, at some critical value of $\eta = \eta_c$, the strength of the hybridization may become strong enough so that the ground state will change from the A_{1g} to the B_{1g} pairing symmetry.

To support this argument, we plot in Figs. 11(c) and (d) the superconducting order parameters⁴⁶ on the Fermi surfaces of the coupled Fe-based ladders in the folded Brillouin zone at two typical values of η . We have used the same exchange constants ($J_1 = 0$ and $J_2 = 0.1D$) as in Fig. 8, where the symmetry change occurs at $\eta_c \approx 0.41$. For $\eta = 0.6 > \eta_c$, the system retains the A_{1g} symmetry of the isotropic planes [Fig. 11(c)]. But the gap amplitudes are significantly reduced due to the hybridization. For $\eta = 0.3 < \eta_c$, the Fermi surface pockets are more one-dimensional as compared to those at $\eta = 0.6$. Eventually they will become straight lines along k_y and the electron pocket at X will disappear when η approaches 0, as shown in Fig. 2. More importantly for our discussion, the dominant pairing channel now has the B_{1g} symmetry, with the gap nodes appearing on the hybridized hole pockets [Fig. 11(d)]. However, contrary to the common expectation from Fig. 11(b), the superconducting order parameters have the same sign on the two hybridized electron pockets. This peculiar gap structure simply manifests the fact that A_{1g} and B_{1g} are not rigorous representations for the ladder system without the D_{4h} symmetry so that different symmetry components are always mixed. In our model, it is the gap structure on the hybridized hole pockets that determines the leading pairing symmetry of the whole system, which we identify as A_{1g} for $\eta > \eta_c$ and B_{1g} for $\eta < \eta_c$.

Furthermore, we can apply the same argument to the cuprates and understand why the d -wave pairing symmetry is favored in both Cu planes and ladders. For the Fermi surface topology of the cuprates, the largest gap amplitude appears at the anti-nodal regions, $(\pm\pi, 0)$ and $(0, \pm\pi)$. Because these regions do not overlap with each other upon folding along $k_y = \pm\pi/2$, the hybridization does not cost significant energy despite of the sign change of the superconducting order parameters. Consequently, the dominant pairing symmetry remains d -wave as the Cu plane is decoupled into the two-leg ladders.

Such a change of the pairing symmetry induced by the hybridization effect has been considered previously^{47,48} in the context of KFe_2Se_2 , where the hybridization occurs between the two electron pockets. In particular, Ref. 48 shows that as the strength of the hybridization increases, the system goes from d -wave to s -wave, with an intermediate $s+id$ state. This issue of time-reversal sym-

metry breaking is beyond the scope of the current work because the superconducting order parameters are restricted to be real here. However, both phenomenological and microscopic theoretical studies^{49–51} have found that the appearance of the time-reversal symmetry breaking phase, at least at the mean-field level, is very general for systems with competing pairing symmetries. So it is possible that our model may exhibit an intermediate $A_{1g} + iB_{1g}$ mean-field phase as the system dimension is reduced from planes to ladders.

In conclusion, we have studied the superconducting phase diagram of a three-orbital t - J model defined on two-leg ladders motivated by the recently discovered ladder iron selenides superconductors. In contrast to the A_{1g} state found in the two-dimensional Fe planes, the favorable pairing channel in the case of the Fe-based ladders

studied here has the B_{1g} symmetry, which is characterized by the opposite signs of the superconducting order parameters on the d_{xz} and d_{yz} orbitals. Furthermore, by investigating the dimensional crossover from planes to ladders, we have found that the system undergoes a first-order transition between the two competing phases. This change of the pairing symmetry may also occur continuously, with an intermediate $A_{1g} + iB_{1g}$ state that breaks the time-reversal symmetry.

ACKNOWLEDGMENTS

This work was supported by the National Science Foundation Grant No. DMR-1104386.

-
- ¹ D. J. Scalapino, Rev. Mod. Phys. **84**, 1383 (2012).
² I. I. Mazin, D. J. Singh, M. D. Johannes, and M. H. Du, Phys. Rev. Lett. **101**, 057003 (2008).
³ K. Kuroki, S. Onari, R. Arita, H. Usui, Y. Tanaka, H. Kontani, and H. Aoki, Phys. Rev. Lett. **101**, 087004 (2008).
⁴ S. Graser, T. A. Maier, P. J. Hirschfeld, and D. J. Scalapino, New Journal of Physics **11**, 025016 (2009).
⁵ F. Wang, H. Zhai, Y. Ran, A. Vishwanath, and D.-H. Lee, Phys. Rev. Lett. **102**, 047005 (2009).
⁶ A. V. Chubukov, D. V. Efremov, and I. Eremin, Phys. Rev. B **78**, 134512 (2008).
⁷ V. Cvetkovic and Z. Tesanovic, EPL (Europhysics Letters) **85**, 37002 (2009).
⁸ Q. Si and E. Abrahams, Phys. Rev. Lett. **101**, 076401 (2008).
⁹ K. Seo, B. A. Bernevig, and J. Hu, Phys. Rev. Lett. **101**, 206404 (2008).
¹⁰ W.-Q. Chen, K.-Y. Yang, Y. Zhou, and F.-C. Zhang, Phys. Rev. Lett. **102**, 047006 (2009).
¹¹ P. Goswami, P. Nikolic, and Q. Si, EPL (Europhysics Letters) **91**, 37006 (2010).
¹² A. Nicholson, W. Ge, X. Zhang, J. Riera, M. Daghofer, A. M. Oleś, G. B. Martins, A. Moreo, and E. Dagotto, Phys. Rev. Lett. **106**, 217002 (2011).
¹³ S.-P. Kou, T. Li, and Z.-Y. Weng, EPL (Europhysics Letters) **88**, 17010 (2009).
¹⁴ J. Dai, Q. Si, J.-X. Zhu, and E. Abrahams, Proceedings of the National Academy of Sciences **106**, 4118 (2009).
¹⁵ W. Lv, F. Krüger, and P. Phillips, Phys. Rev. B **82**, 045125 (2010).
¹⁶ W.-G. Yin, C.-C. Lee, and W. Ku, Phys. Rev. Lett. **105**, 107004 (2010).
¹⁷ P. Dai, J. Hu, and E. Dagotto, Nature Physics **8**, 709 (2012).
¹⁸ R. Yu and Q. Si, Phys. Rev. Lett. **110**, 146402 (2013).
¹⁹ K. Okazaki, Y. Ota, Y. Kotani, W. Malaeb, Y. Ishida, T. Shimojima, T. Kiss, S. Watanabe, C.-T. Chen, K. Kihou, C. H. Lee, A. Iyo, H. Eisaki, T. Saito, H. Fukazawa, Y. Kohori, K. Hashimoto, T. Shibauchi, Y. Matsuda, H. Ikeda, H. Miyahara, R. Arita, A. Chainani, and S. Shin, Science **337**, 1314 (2012).
²⁰ R. Thomale, C. Platt, W. Hanke, J. Hu, and B. A. Bernevig, Phys. Rev. Lett. **107**, 117001 (2011).
²¹ K. Suzuki, H. Usui, and K. Kuroki, Phys. Rev. B **84**, 144514 (2011).
²² S. Maiti, M. M. Korshunov, and A. V. Chubukov, Phys. Rev. B **85**, 014511 (2012).
²³ M. Xu, Q. Q. Ge, R. Peng, Z. R. Ye, J. Jiang, F. Chen, X. P. Shen, B. P. Xie, Y. Zhang, A. F. Wang, X. F. Wang, X. H. Chen, and D. L. Feng, Phys. Rev. B **85**, 220504 (2012).
²⁴ C. Fang, Y.-L. Wu, R. Thomale, B. A. Bernevig, and J. Hu, Phys. Rev. X **1**, 011009 (2011).
²⁵ R. Yu, P. Goswami, Q. Si, P. Nikolic, and J.-X. Zhu, (2011), arXiv:1103.3259.
²⁶ T. A. Maier, S. Graser, P. J. Hirschfeld, and D. J. Scalapino, Phys. Rev. B **83**, 100515 (2011).
²⁷ F. Wang, F. Yang, M. Gao, Z.-Y. Lu, T. Xiang, and D.-H. Lee, EPL (Europhysics Letters) **93**, 57003 (2011).
²⁸ E. Dagotto, Rev. Mod. Phys. **85**, 849 (2013).
²⁹ W. Li, H. Ding, P. Zhang, P. Deng, K. Chang, K. He, S. Ji, L. Wang, X. Ma, J. Wu, J.-P. Hu, Q.-K. Xue, and X. Chen, (2012), arXiv:1210.4619.
³⁰ J. M. Caron, J. R. Neilson, D. C. Miller, A. Llobet, and T. M. McQueen, Phys. Rev. B **84**, 180409 (2011).
³¹ H. Lei, H. Ryu, A. I. Frenkel, and C. Petrovic, Phys. Rev. B **84**, 214511 (2011).
³² Y. Nambu, K. Ohgushi, S. Suzuki, F. Du, M. Avdeev, Y. Uwatoko, K. Munakata, H. Fukazawa, S. Chi, Y. Ueda, and T. J. Sato, Phys. Rev. B **85**, 064413 (2012).
³³ J. M. Caron, J. R. Neilson, D. C. Miller, K. Arpino, A. Llobet, and T. M. McQueen, Phys. Rev. B **85**, 180405 (2012).
³⁴ E. Dagotto, J. Riera, and D. Scalapino, Phys. Rev. B **45**, 5744 (1992).
³⁵ M. Sigrist, T. M. Rice, and F. C. Zhang, Phys. Rev. B **49**, 12058 (1994).
³⁶ E. Dagotto and T. M. Rice, Science **271**, 618 (1996).
³⁷ E. Dagotto, Reports on Progress in Physics **62**, 1525 (1999).
³⁸ Note that s -wave and d -wave are not the appropriate notations in the ladder system. But we will use them throughout the paper by analogy with the two-dimensional system.
³⁹ W. Li, C. Setty, X. H. Chen, and J. Hu, (2012), arXiv:1202.4016.

- ⁴⁰ Q. Luo, A. Nicholson, J. Rincón, S. Liang, J. Riera, G. Alvarez, L. Wang, W. Ku, G. D. Samolyuk, A. Moreo, and E. Dagotto, *Phys. Rev. B* **87**, 024404 (2013).
- ⁴¹ P. A. Lee and X.-G. Wen, *Phys. Rev. B* **78**, 144517 (2008).
- ⁴² M. J. Calderón, B. Valenzuela, and E. Bascones, *Phys. Rev. B* **80**, 094531 (2009).
- ⁴³ M. Daghofer, A. Nicholson, A. Moreo, and E. Dagotto, *Phys. Rev. B* **81**, 014511 (2010).
- ⁴⁴ W. Lv and P. Phillips, *Phys. Rev. B* **84**, 174512 (2011).
- ⁴⁵ J. Hu and H. Ding, *Sci. Rep.* **2**, 381 (2012).
- ⁴⁶ Note that only the dominant intra-band superconducting order parameters are plotted. In general, both intra-band and inter-band pairings are present after the transformation from the orbital to band basis. See A. Moreo, M. Daghofer, A. Nicholson, and E. Dagotto, *Phys. Rev. B* **80**, 104507 (2009).
- ⁴⁷ I. I. Mazin, *Phys. Rev. B* **84**, 024529 (2011).
- ⁴⁸ M. Khodas and A. V. Chubukov, *Phys. Rev. Lett.* **108**, 247003 (2012).
- ⁴⁹ W.-C. Lee, S.-C. Zhang, and C. Wu, *Phys. Rev. Lett.* **102**, 217002 (2009).
- ⁵⁰ V. Stanev and Z. Tešanović, *Phys. Rev. B* **81**, 134522 (2010).
- ⁵¹ S. Maiti and A. V. Chubukov, *Phys. Rev. B* **87**, 144511 (2013).